Title: Shortwave radiation experiments in HARMONIE. Tests of the cloud inhomogeneity factor and a new cloud liquid optical property scheme compared to observations

Author(s): Gleeson, E.,[1] Nielsen, K.P., [2] Toll, V.,[3] Rontu, L.[4] & Whelan, E.[1]

[1] Danish Meteorological Institute, Lyngbyvej 100, 2100, Copenhagen, Denmark
[2] Met Éireann, Glasnevin Hill, Dublin, Ireland
[3] Institute of Physics, University of Tartu, Tartu, Estonia
[4] Finnish Meteorological Institute, Meteorological Research, Box 503, 00101 Helsinki.

Citation: Gleeson, E. et al., 2015. Shortwave radiation experiments in HARMONIE. Tests of the cloud inhomogeneity factor and a new cloud liquid optical property scheme compared to observations. *ALADIN-HIRLAM Newsletter*, 5, pp.92–106.

Shortwave Radiation Experiments in HARMONIE

Tests of the cloud inhomogeneity factor and a new cloud liquid optical property scheme compared to observations

Emily Gleeson, Kristian Pagh Nielsen, Velle Toll, Laura Rontu, Eoin Whelan

1 Introduction

Within the European Union, at least 20% of each country's total energy consumption must come from renewable sources by the year 2020, increasing to at least 27% by 2030. Solar energy is currently one of the least expensive forms of clean energy. With the growing interest in and use of solar power comes the need for reliable solar or shortwave (SW) radiation forecasts.

SW radiation strongly impacts on weather at the Earth's surface and the development of the atmospheric boundary layer. Thus, improvements in the representation of SW radiation are important for the ongoing improvement of numerical weather prediction (NWP) forecasts. Accurate SW radiation output from NWP models relies on the accuracy of **1.** cloud cover, **2.** the physical properties of clouds (liquid water load, ice water load, effective water and ice radii), **3.** the optical properties of the clouds, **4.** the radiative transfer approximations and **5.** aerosols and atmospheric gases. In this study, we mainly focus on 2 and 3, the influence of the physical and optical properties of clouds.

Regarding aerosols (**5**), HARMONIE uses monthly climatologies of vertically integrated aerosol optical depth (AOD) at 550nm (Tegen et al., 1997). The aerosol optical properties (single scattering albedo (SSA), assymetry factor (g) and AOD scaling for each SW radiation band) are parametrized following Hess et al. (1998). Toll et al. (2015) found a noticeable improvement in the HARMONIE NWP forecast for a heavily polluted Russian wildfire case study when the direct radiative effect of the real time aerosol distribution was used instead of the climatological distribution. For situations where the aerosol distributions are close to average, updating the aerosol climatology or using real time aerosol distributions only results in small improvements (Toll et al., in preparation). The indirect radiative effect of aerosols in HARMONIE has not yet been extensively studied.

The radiative transfer approximations (**4**) have been extensively tested by Nielsen et al. (2014) using MUSC, the single column version of HARMONIE. In that study, the SW radiation schemes in the model were compared to the accurate DISORT model run within the libRadtran framework (Stamnes et al., 1988, 2000; Mayer and Kylling, 2005) for a range of clear sky, cloud liquid and cloud ice experiments. The benchmark tests included a study of the cloud inhomogeneity factor, the current SW cloud liquid optical property parametrizations available in HARMONIE (Fouquart, 1987 and Slingo 1989) and a new parametrization proposed by Nielsen.

The present study using 3D HARMONIE expands on the 1D benchmark tests done using MUSC. Here we focus on the influence of the cloud inhomogeneity factor, which effectively modifies the cloud water and ice loads used in the radiation calculations, and the new Nielsen cloud liquid optical property scheme on forecasts for the Irish operational domain.

Regarding the cloud inhomogeneity factor, there are several studies that try to quantify the radiative response of the inhomogeneity of different cloud types using observations (e.g. Pomroy and Illingworth, 2000; Hogan and Illingworth, 2003). Oreopoulos and Cahalan (2005) have investigated the climatology of cloud inhomogeneity using MODIS data.

Subgrid scale variability in cloud properties induces errors in simulated longwave (LW) and SW radiative fluxes in global climate model simulations when this variability is not accounted for (Scheirer and Macke, 2003; Fu et al., 2000). The relationships between both SW albedo and LW emissivity and cloud optical thickness are nonlinear so that inhomogeneous clouds have a lower mean SW albedo and a lower mean LW emissivity than homogeneous clouds with the same mean optical thickness. The inhomogeneity parameter χ is defined as the ratio of the exponential of the logarithmic average of the cloud optical thickness to the linear average of the cloud optical thickness (Equation 1). This parameter can be used as a good approximation of the effective optical thickness in the case of inhomogeneous clouds (Oreopoulos et al. 2005; Cahalan et al. 1994).

$$\chi = \frac{e^{\overline{\ln \tau}}}{\overline{\tau}} \quad (1)$$

In the current SW and LW radiation schemes used by default in the HARMONIE model (Seity et al., 2011, Brousseau et al., 2011) an inhomogeneity correction factor has been used to scale the cloud optical thickness (cloud water and ice loads) to account for subgrid cloud variability following Tiedtke (1996). A value of 0.7 was chosen following an observational study by Cahalan et al. (1994). This inhomogeneity factor and the radiation parametrizations originate from cycle 25R1 of the ECMWF global model IFS (see ECMWF, 2012 and Mascart and Bougeault, 2011). Tiedtke (1996) showed that this cloud inhomogeneity factor led to a 9 W/m^2 increase in the average net downward SW radiation flux over tropical oceans.

In HARMONIE deep convection is treated explicitly at the default horizontal grid spacing of 2.5km. In addition, cloud structure is better resolved compared to the global IFS model which has coarser grid spacing (T511 or ~40km grid spacing was used in the IFS model at the time when the cloud inhomogeneity factor was introduced). Consequently, it is not physically correct to use a correction factor of 0.7 for cloud optical thickness in HARMONIE at high horizontal resolution (pers. comm. Hogan 2014 unpublished Townsend dissertation 2015) and in this study we investigate the effect of this inhomogeneity factor on HARMONIE NWP forecasts for Ireland and the UK.

In Nielsen et al. (2014) the Nielsen scheme was shown to be better than the Fouquart and Slingo schemes for a suite of 1D cloud liquid tests. The new scheme was developed because initial tests of the Fouquart and Slingo cloud liquid optical property schemes in HARMONIE showed significant deviations from the Mie calculations. The new Nielsen scheme is based on empirical fits to the Mie calculations (see Nielsen et al., 2014 Supplement 1). To complete the validation of the scheme, 3D experiments were carried out and are presented here.

The final part of this study involved using downward global SW radiation as a proxy for cloudiness by computing the clear sky index (downward global SW radiation normalised by the clear sky downward SW radiation) and the evaluation of HARMONIE cloud cover and cloud condensate compared with MSGCPP satellite data (Roebeling et al., 2006). Perez et al. (2014) performed a detailed analysis of the HARMONIE cloud cover forecasts. They also discussed the diagnosis of cloud cover variability in terms of the three-dimensional fractional cloud cover defined in each gridbox. Three-dimensional fractional cloud cover is also used by the radiation parametrizations to derive the grid-scale cloud condensate load from the cloud liquid and ice content given by the microphysics parametrizations. The analysis that we show here is complementary to the analysis of Perez et al. (2014) in that we also analyse the cloud condensate load, which can vary independently from the cloud cover.

2 HARMONIE Set-up and Experiments

HARMONIE cycle 38h1.2 on a 2.5km horizontal grid, with 540x500 grid-points in the x- and y-directions and 65 hybrid model levels (Simmons and Burridge 1981; Laprise 1992), was used for the experiments described in this article. The model domain was centred over the island of Ireland and includes the UK and part of northern France.

Lateral boundary conditions from the ERA-Interim re-analysis project (Dee et al., 2011) at a 3-hour frequency were used. Observations, retrieved from ECMWF's MARS archive and Met Éireann's observation database, were assimilated using the model's three-dimensional variational (3DVAR) data assimilation system (with no digital filtering). Observations from land surface stations, ships and drifting buoys, radiosonde ascents and aircraft were assimilated. Surface observations were also assimilated in the model's surface analysis system using optimal interpolation. The experiments were configured to use a 3 hourly cycling strategy with a 1.5 hour observation window.

This body of work includes 3 radiation experiments. The default SW radiation scheme in HARMONIE is the IFS scheme (ECMWF cycle 25R1) with six SW spectral bands, three in the ultraviolet/visible spectral range and three in the solar infrared range (Mascart and Bougeault, 2011). The delta-Eddington approximation (Joseph et al., 1976; Fouquart and Bonnel, 1980) is used for the radiative transfer calculations with the cloud liquid and cloud ice optical properties calculated with the Fouquart (1987) and the Ebert and Curry (1992) parametrizations respectively. Before being used for radiation calculations the cloud water load is modified by so-called cloud SW and cloud LW inhomogeneity factors, each of which is set to 0.7 in the default set-up.

Figure 1. *Map of Ireland showing the locations of the shortwave radiation measurement sites.*

In addition to the default IFS SW radiation scheme (REFEXP), we ran 2 comparison experiments (INHOMEXP, COPEXP). In the first of these (INHOMEXP), we set both the cloud SW and cloud LW inhomogeneity factors to 1.0 as the current default values of 0.7 were set for IFS model versions with horizontal grid spacings of ~10-100km. HARMONIE is run on a 2.5km grid. At this grid spacing sub-grid cloud inhomogeneity has a smaller effect on the average cloud optical thickness. Thus, we suggest inhomogeneity factors of 1.0 instead (Nielsen et al., 2014). In the second experiment (COPEXP), we used a new cloud liquid optical property scheme (the Nielsen scheme, Nielsen et al., 2014). The default cloud ice optical property scheme and the delta-Eddington approximation for radiative transfer

were still used. Both the cloud SW and LW inhomogeneity factors were set to 1 as in the previous experiment. Therefore, COPEXP is identical to REFEXP except for changes to the cloud liquid optical property scheme and the inhomogeneity factors in the radiation parametrization.

Two month-long simulations were carried out: June and December 2013, with each having a 10-day spin-up period during the previous month. 48-hour forecasts were run at 00 and 12 UTC with 3-hour forecasts run at each of the remaining cycles for data assimilation continuity.

In HARMONIE's Webgraf verification package observations from synoptic stations and upper-air soundings covering the domain were used. SW radiation observations from 7 synoptic stations in Ireland (Belmullet, Clones, Dublin Airport, Gurteen, Johnstown Castle, Malin Head, Valentia – see Figure 1) and MSGCPP cloud cover and cloud condensate data were also used to verify the output from HARMONIE.

3 Results and Discussion

The results are presented in four sections, focusing on June 2013 because during this period the investigated effects (difference in cloud inhomogeneity, cloud liquid optical property scheme) induced changes. This was expected as the changes are predominantly SW radiation-related and during December in Ireland, SW radiation is significantly lower than in June.

Forecast verification using observations recorded at synoptic stations and from upper-air ascents (for stations in the experiment domain) is presented in Section 3.1. Section 3.2 shows areal comparisons of relevant output from the experiments. More detailed analysis of the global SW radiation output from HARMONIE compared to measurements over Ireland is presented in Section 3.3. Finally a comparison of HARMONIE cloud cover and cloud condensate (cloud water and ice) versus MSGCPP satellite data is detailed in Section 3.4.

3.1 Verification versus synoptic station data and radiosondes

The results presented in this section are mainly temperature focused where available observations from synoptic stations and upper-air ascents over the experiment domain are compared to the output from each HARMONIE experiment. Figure 2(a) shows a clear increase of ~0.1 degrees in the negative bias in 2m temperature when the cloud inhomogeneity factor is removed (i.e. set to 1) with a further ~0.1 degree reduction using the Nielsen cloud liquid optical property scheme. INHOMEXP and COPEXP have more negative biases in specific humidity (Figure 2b) and precipitation (Figure 2c) and neutral effects on wind speeds, cloud and mean sea level pressure. Lower temperatures cause less evaporation, lower humidity and less precipitation. However, the statistical significance of these results has not been tested. Figure 3(a,b) shows the decreases in temperature at the 925hPa and 850hPa pressure levels as a function of forecast length, with the decreases more pronounced at the 850hPa level. This is also indicated in the temperature profiles shown in Figure 3(c) which shows the average temperature bias at each pressure level valid at 12 UTC.

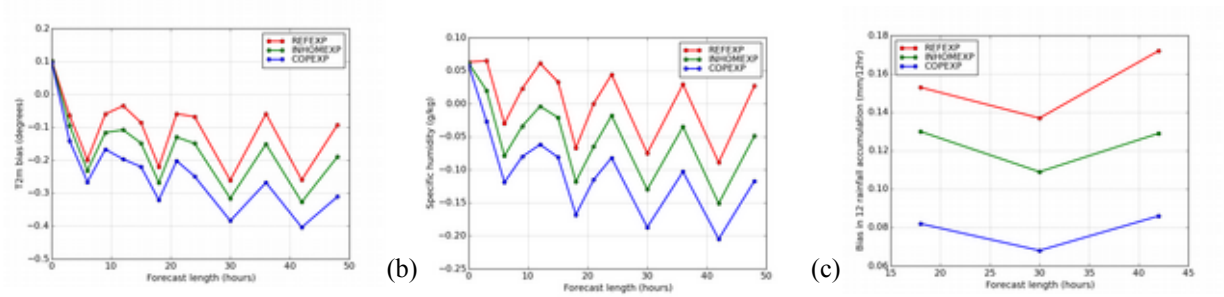

Figure 2. *Bias in (a) 2m temperature, (b) specific humidity and (c) precipitation as a function of forecast length for the REFEXP, INHOMEXP and COPEXP experiments.*

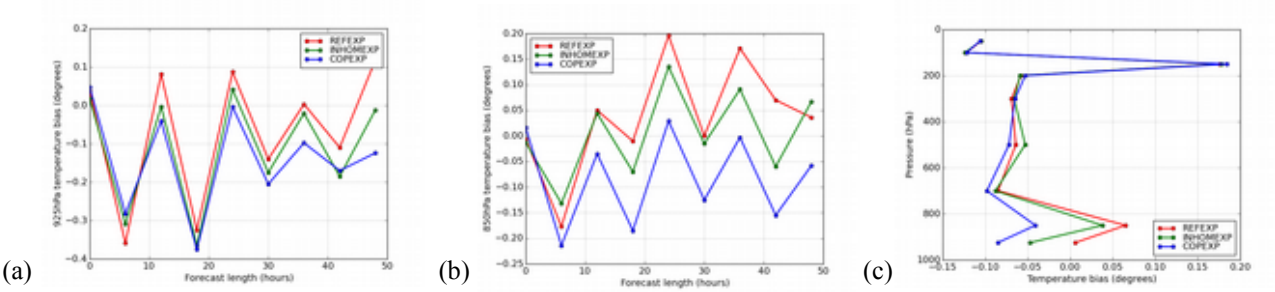

Figure 3. *Bias in (a) 925 hPa and (b) 850 hPa temperature as a function of forecast length (c) bias in temperature at various pressure levels (valid at 12UTC) for the REFEXP, INHOMEXP and COPEXP experiments.*

3.2 Areal comparisons of the INHOMEXP and COPEXP versus REFEXP temperature and energy fluxes

Mean monthly surface temperature over the domain for June 2013 is shown in Figure 4(a) for REFEXP, the default HARMONIE set-up, where hourly forecasts up to 24 hours from each of the 00UTC runs were used in the calculation. The INHOMEXP and COPEXP relative biases compared to REFEXP are shown in Figure 4(b) and 4(c). The biases are mostly negative and more pronounced in COPEXP which includes the effect of having no cloud inhomogeneity as well as the new cloud liquid optical property scheme. As expected, these biases are only over land as sea surface temperatures (SSTs) in the model are derived from ERA-Interim reanalysis data. The lateral boundary conditions are updated at 3-hour intervals, during which time the SSTs vary insignificantly compared to surface temperatures over land. Figure 5(a) shows the mean surface temperature over all land points in the domain for each experiment by time of day at 3-hour intervals, where again forecasts from the 00UTC runs were used in the calculation. Figure 5(b) is similar but shows the biases in surface temperature for INHOMEXP and COPEXP relative to REFEXP. Both figures clearly illustrate the diurnal dependence of the effect of the cloud inhomogeneity and liquid optical property scheme on surface temperatures.

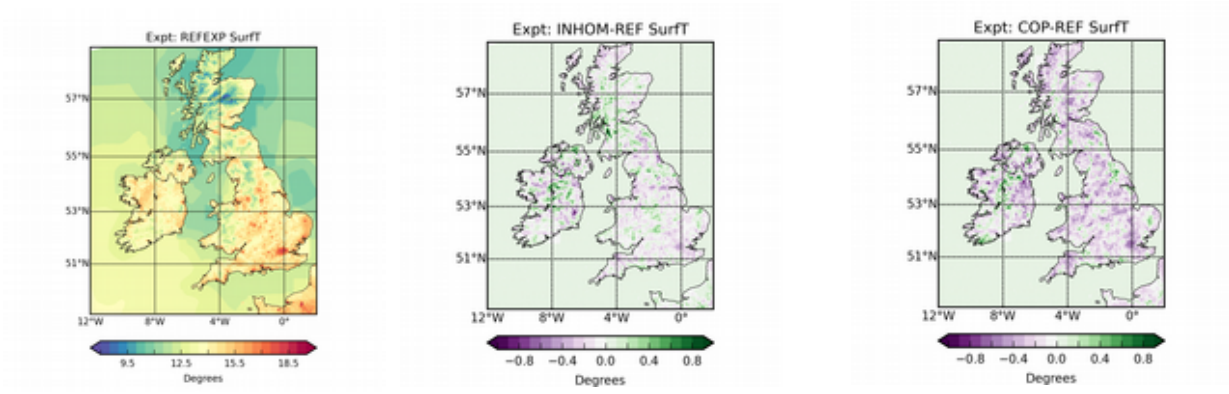

(a) (b) (c)

Figure 4. *(a) REFEXP (b) INHOMEXP minus REFEXP and (c) COPEXP minus REFEXP monthly mean surface temperature. In each case the hourly forecasts (up to 24 hours) from the 00UTC cycles were used.*

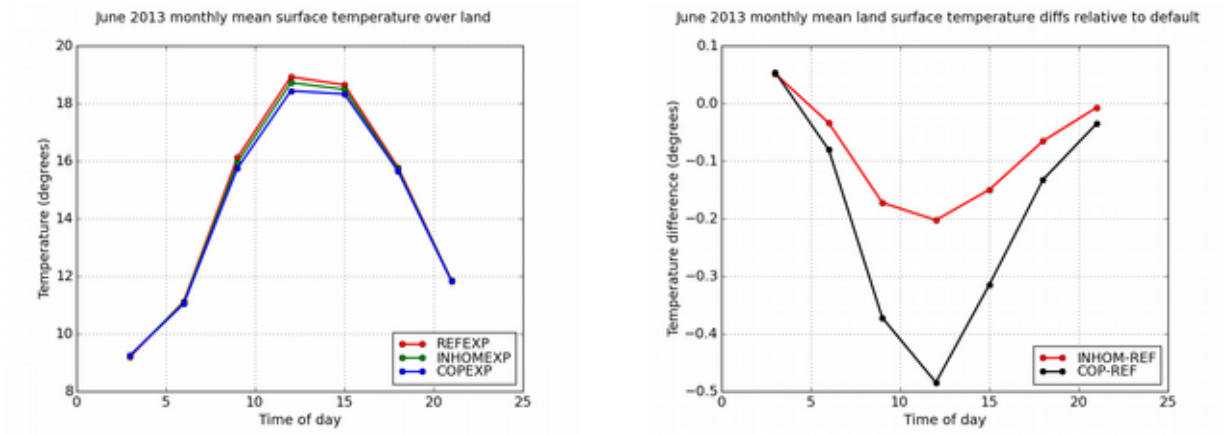

(a) (b)

Figure 5. *(a) Monthly mean surface temperature over all land grid points and at 3-hour intervals during the day, using forecasts from the 00UTC forecast cycles. (b) Similar to (a) but differences relative to the default set-up are plotted.*

Most of these changes in temperature (surface, 2m, lower troposphere below 850hPa) can be explained by the decrease in the downwelling SW radiation flux (SWD) shown in Figure 6. The diurnal cycle of the surface temperature differences and also the differences in this cycle for INHOMEXP and COPEXP can also be attributed to the differences in SWD. The average decrease in SWD over land grid points is 11 W/m^2 for INHOMEXP and 22 W/m^2 for COPEXP. On the other hand, the changes in downwelling LW radiation at the surface (LWD, Figure 7) are an order of magnitude smaller (< 1W/m^2 average change over land grid points for both experiments compared to REFEXP).

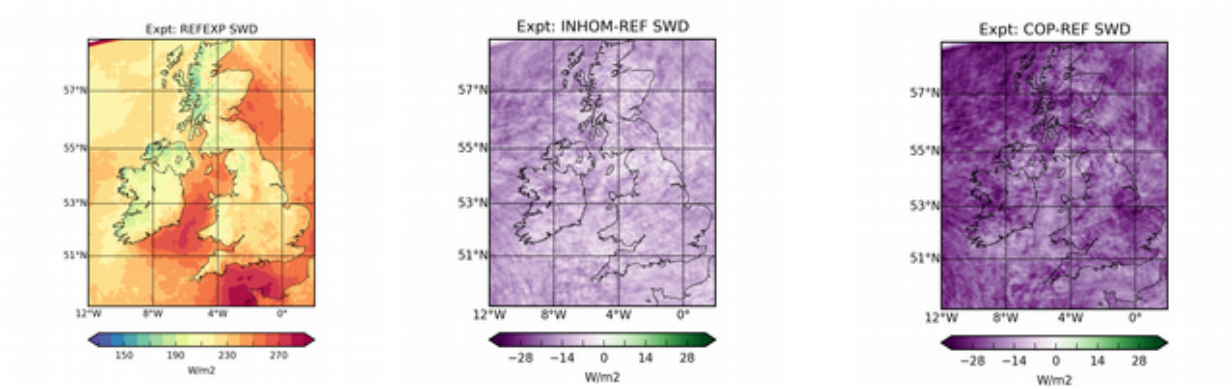

(a) (b) (c)

Figure 6. *(a) REFEXP (b) INHOMEXP minus REFEXP and (c) COPEXP minus REFEXP monthly mean of daily mean global SW radiation. In each case the hourly forecasts (up to 24 hours) from the 00UTC cycles were used.*

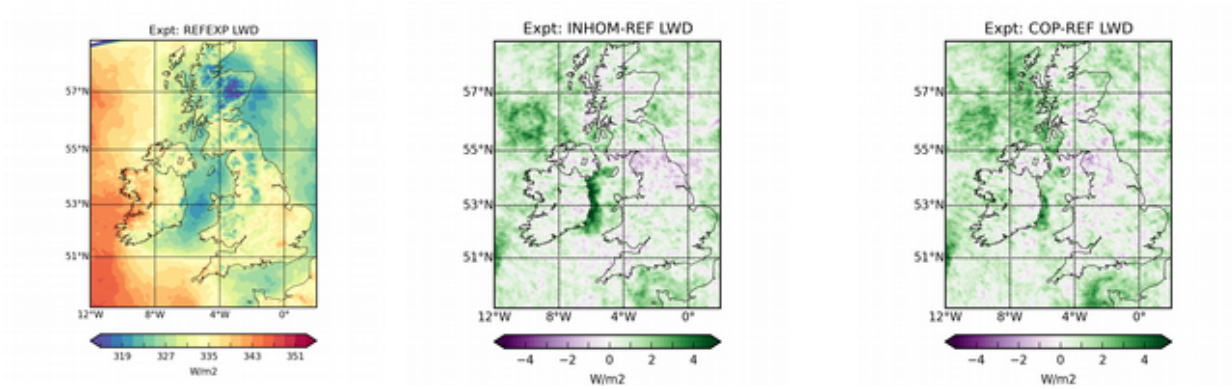

(a) (b) (c)

Figure 7. *(a) REFEXP (b) INHOMEXP minus REFEXP and (c) COPEXP minus REFEXP monthly mean of daily mean downwelling LW radiation at the surface. In each case the hourly forecasts (up to 24 hours) from the 00UTC cycles were used.*

3.3 Downwelling SW Radiation Verification and the Clear Sky Index (CSI)

In this section we focus on downwelling global SW radiation in more detail comparing hourly accumulations of SWD at 7 synoptic stations (Figure 1) in Ireland to HARMONIE output for the 3 experiments for June 2013. The clear sky index is a useful parameter for comparing SW radiation because it also acts as a proxy for cloud cover and cloud condensate amounts. The index is the ratio of global SWD divided by the maximum possible global SWD and is dependent on the location, date and time. In this case, the index was computed using observations from the 7 Irish stations and data from the 3 HARMONIE experiments, bi-linearly interpolated to the station locations. At each location, and for the observations and HARMONIE experiments separately, the CSI was computed using the average solar zenith angle (SZA) over the previous hour. The average SZA over the previous hour was used because the accumulations of SWD are available at hourly intervals in HARMONIE. For computational reasons it was not possible to output and store data at a time resolution of one minute. Hence, since hourly averages of SWD are used in the CSI calculations, the hourly average SZA for the same period was also used.

It is important to note that the clear sky irradiances from HARMONIE were not used; instead the maximum solar irradances were computed separately using locations, dates and times. These were computed using the hlsolar.F90 solar astronomy subroutine from HiRLAM and our newly tuned version of the Savijärvi et al., 1990 clear sky equation (Equation 2) for global SW radiation at the surface using a 2.5 g/cm² water vapour load. We tuned constants *C1*, *C2* and *C3* using the clear sky experiments discussed in Nielsen et al., 2014 where *C1* and *C2* are associated with integrated water vapour *u* and C3 is associated with backscattering from reflected beams. *C1*, *C2* and *C3* are 0.11, 0.25 and 0.07 respectively. S_0 is the solar irradiance at the top of atmosphere, which varies with the Sun-Earth distance, and *h* is the angular solar height.

$$S(sfc) = S_0 \sin(h)\left(1 - 0.024\sin(h)^{-0.5} - C1\left(\frac{u}{\sin(h)}\right)^{C2} - \left(\frac{0.28}{1+6.43\sin(h)} - C3\alpha\right)\right) \quad (2)$$

This approach was taken because only instantaneous clear sky SW fluxes at the surface are available in HARMONIE but accumulated fluxes are required. A water vapour load of 2.5 g/cm² was used as it is a typical value at midlatitudes. For low water vapour loads the clear sky irradiances will be approximately 10% higher, as was shown in Nielsen et al. (2014). A 10% difference does not affect the results strongly. For greater accuracy, modelled water vapour loads and the water vapour loads from MSGCPP should be used in the HARMONIE and observed CSI calculations respectively.

To aid analysis the data were then binned by CSI and hourly mean cosine of the SZA. Data from the 7 Irish stations were amalgamated to produce Figure 8, where SWD biases relative to observations are plotted. The CSI (observation data) and cos(SZA) bins are each in steps of 0.1. Cos(SZA) is denoted negative when the solar azimuthal angle is negative (i.e. the Sun is in the eastern sky) to investigate whether the positioning of the Sun has an obvious effect on the biases. CSI values greater than 1 mainly occur at low SZAs and can also be caused by optically enhancing sun cloud geometries. The reduction in global SW radiation can be clearly seen when the inhomogeneity factor is increased from its default value of 0.7 to 1.0 (i.e. less transparent clouds) and further still when the Nielsen SW cloud liquid optical property scheme is used. These biases are explored in more detail in Figures 9-11. Subsets of the data in Figure 8 are plotted in Figure 9 where typical CSI ranges (0.4 to 0.5 and also 0.5 to 0.6) were selected. In each case, the decrease in SWD relative to REFEXP is greater for higher SZAs. This effect is more pronounced in the CSI=0.5 to 0.6 case.

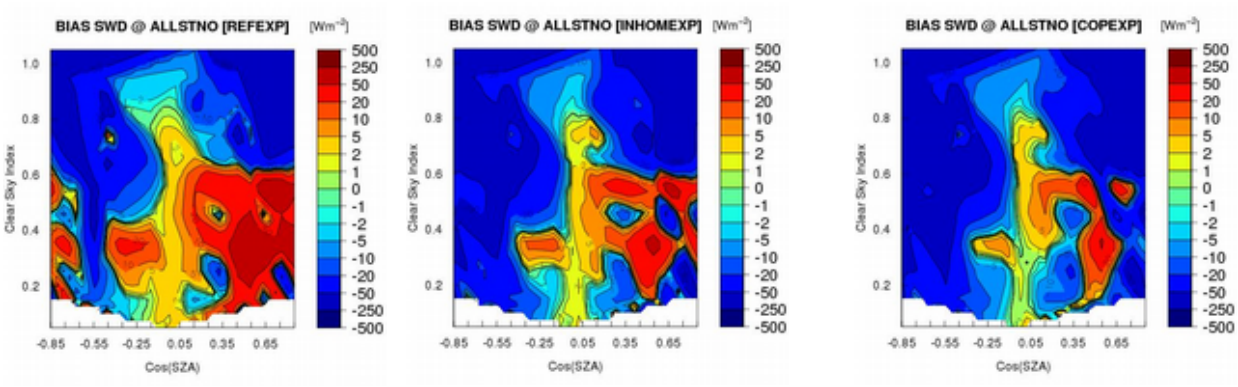

(a) (b) (c)

Figure 8. *(a) REFEXP (b) INHOMEXP and (c) COPEXP mean bias in global SW radiation compared to measurements at 7 Irish stations where the data are binned by CSI and hourly mean cos(SZA). cos(SZA) is denoted negative when the solar azimuthal angle is negative (i.e. the sun is in the eastern sky). Only data where N>10 (i.e. number of data points per bin >10) are shown and CSI refers to the CSI of the observation data.*

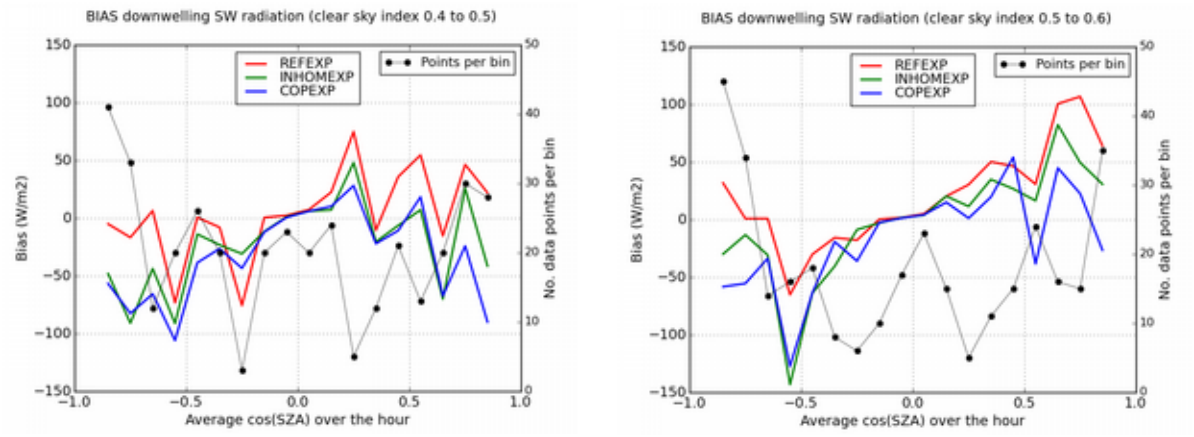

(a) (b)

Figure 9. *Mean bias in global SW radiation compared to measurements at 7 Irish stations where the data are binned by hourly mean cos(SZA) for (a) CSI between 0.4-0.5 and (b) CSI between 0.5-0.6.*

In Figures 8 and 9 the CSI refers to the clear sky index calculated using the observation data. In Figure 10, the CSI for the observations and also the CSIs for each of the 3 radiation experiments are used to generate probability density functions of CSI. We can use these to draw conclusions about cloudiness in the HARMONIE model.

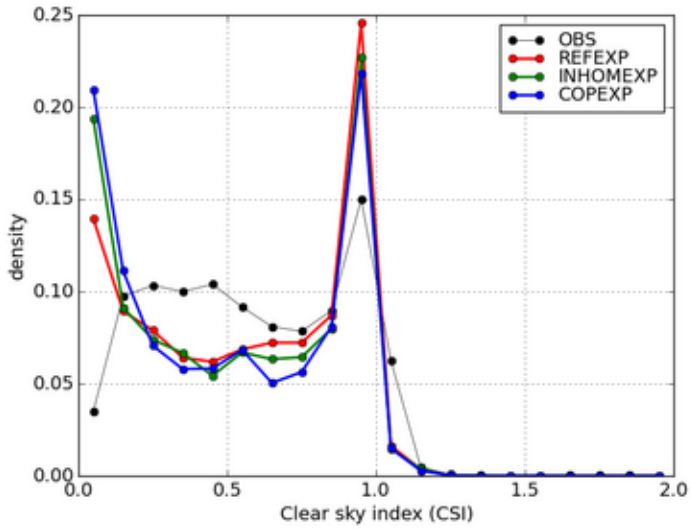

Figure 10. *Probability density functions of CSI using hourly SW observations and forecast data for June 2013 valid at 7 Irish observation locations. Only data where cos(SZA) >0 are included. Observations (black), REFEXP (red), INHOMEXP (green), COPEXP(blue).*

The binary distribution of the CSI (peaks at 0 and 1) gives complementary information to the binary cloud cover shown by Perez et al. (2014). In general the CSI is close to 1 under clear sky conditions. However, the CSI may also be high for cases with 100% cover when the clouds are thin. The main explanation for the results in Figure 10 is that the cloud water loads are too high in the HARMONIE model – this is discussed and illustrated in more detail in Section 3.4. We do not think that the binary cloud issue is due to 3D cloud cover or the overlap assumptions (see Section 3.4). We think that there is too much cloud water in the thickest clouds, and for thick clouds cloud overlap is not really an issue.

3.4 Cloud Water Path and Cloud Cover compared to MSGCPP Satellite Data

As described in the introduction the accuracy of SW radiation forecasts depends on a chain of parameters that include cloud cover, cloud water load, cloud liquid water and ice effective radii and cloud optical properties. In order to determine which of these explain the model issues shown in Figure 10, we performed separate tests of the modelled cloud cover and cloud water loads against MSGCPP SAF products from EUMETSAT. Here the cloud water load is the vertically integrated cloud liquid water and cloud ice.

The mean cloud cover for July 2013 for each of the HARMONIE experiments is over-predicted compared to the MSG cloud cover (not shown). However, the diagnostic cloud cover in HARMONIE is different to the radiative cloud cover as the former uses a random overlap algorithm as opposed to maximum overlap for clouds used in the radiation schemes. The diagnostic cloud cover is higher than the maximum overlap cloud cover (per. comm. Lisa Bengtsson, June 2015). Due to this, we do not know whether the cloud cover in HARMONIE is biased relative to MSG data. In the tests of cloud cover we do not see significant differences between the results of the three HARMONIE experiments.

The second important physical cloud parameter is cloud water load or path (CWP). The monthly mean CWP is shown in Figure 11 (a)-(d) for the three HARMONIE experiments and the MSGCPP satellite derived product. Only data between 07 and 17 UTC (06.45 to 16.45 for MSG) were used. In addition to this, only times where both MSGCPP and HARMONIE have full cloud cover were included, so that the result applies to cloudy cases. It is clear from Figure 11 that HARMONIE, regardless of cloud liquid optics and inhomogeneity, over-predicts cloud condensate, with Figure 11 (e)-(g) showing the HARMONIE biases relative to MSGCPP which are mostly in excess of $0.1 g/m^2$. It is also clear that there are no significant differences in CWP between the three HARMONIE experiments.

Finally Figure 12 focuses on SW radiation biases relative to Irish station data for cases where the observed MSG cloud cover is 1 and the HARMONIE cloud cover exceeds 0.9 with these cloud cover criteria applied to each of the 7 stations separately. Figure 12(a) is a density plot of SWD biases for cloudy cases where data for each of the 7 stations were included to generate the figure; hence in this plot the data are not binned by CWP bias relative to MSG. The SWD biases are clearly skewed towards negative biases, consistent with positive biases in CWP. This is also illustrated in the Figure 12(b) scatter plot of the HARMONIE SW biases relative to station observations versus CWP biases relative to MSG data where again data for each of the 7 stations are amalgamated. The results for the REFEXP are shown here. The red curve with error bars shows the mean +/- the standard deviation of the CWP bias for SWD bias bins at 50 W/m^2 intervals and the cyan curve shows the percentage of data points in each of the SW bias bins. Most of the SW biases lie in the 0 to -50 W/m^2 range and within this sub-range the SW bias is correlated to the positive bias in CWP.

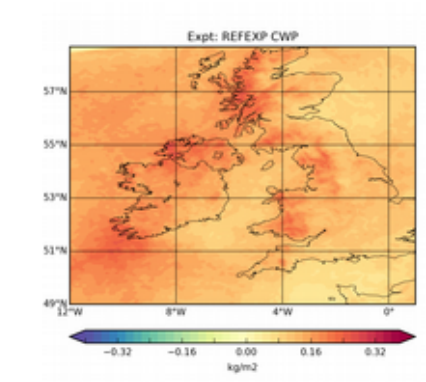

(a)

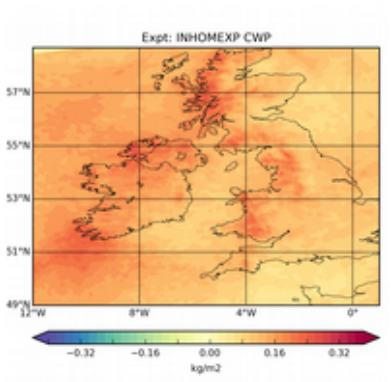

(b)

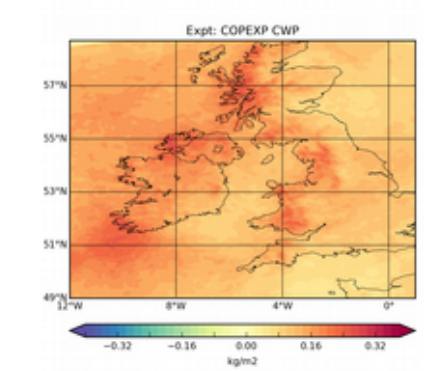

(c)

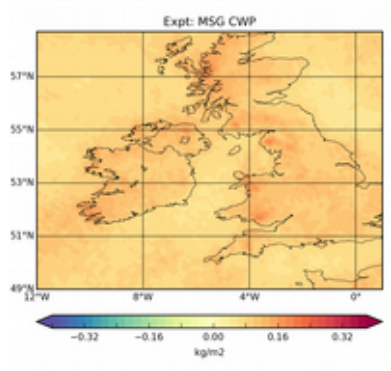

(d)

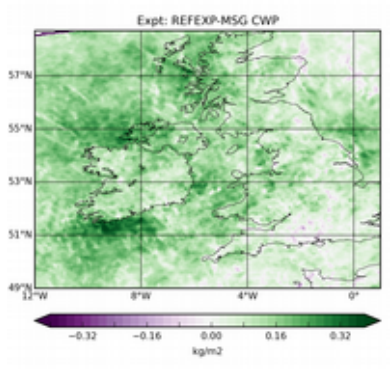

(e)

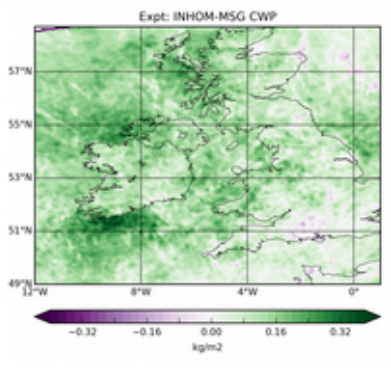

(f)

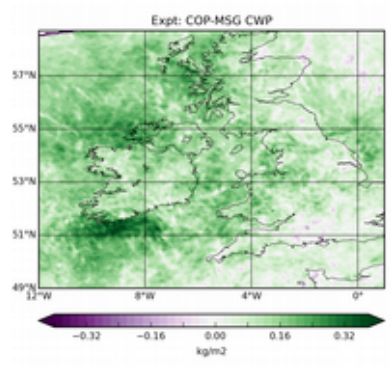

(g)

Figure 11. *Monthly mean instantaneous integrated cloud condensate (water + ice) (kg/m^2) for (a) REFEXP (b) INHOMEXP (c) COPEXP and (d) MSG where data between 07 and 17 UTC were used (i.e. the times for which MSG data were available over the domain). (e), (f), (g) show the HARMONIE minus MSG biases for the REFEXP, INHOMEXP and COPEXP experiments where only grid points where both HARMONIE and MSG have full cloud cover are included.*

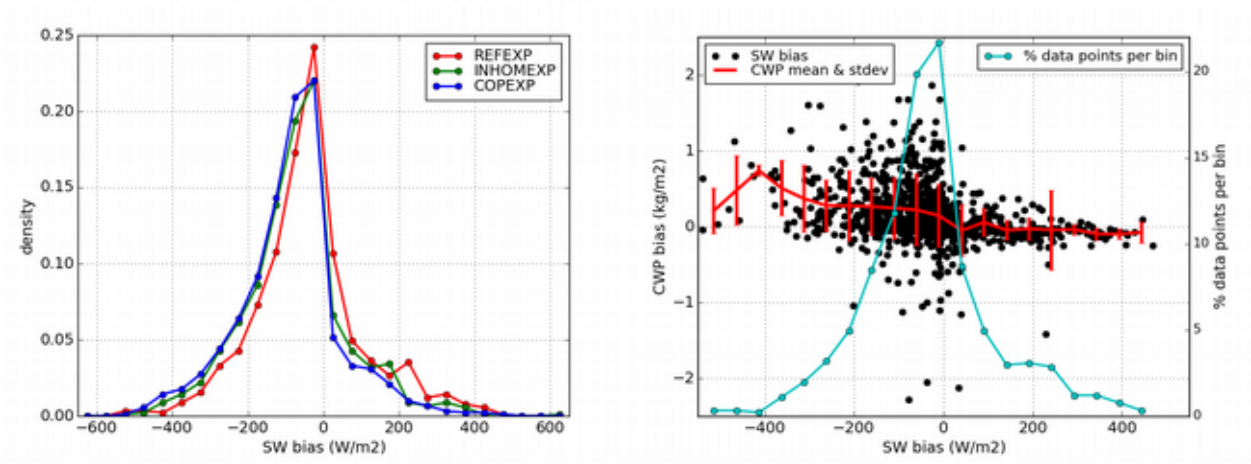

(a) (b)

Figure 12. *(a) SWD bias relative to observations for 7 stations in Ireland for REFEXP, INHOMEXP and COPEXP for cases where MSG has full cloud cover and the cover in HARMONIE is >0.9. (b) Scatter plot of the bias in SWD relative to synoptic station data versus the bias in cloud water path relative to MSG data for the REFEXP. The red bar depicts the mean and standard deviation of the CWP bias for SW bias bins at 50W/m^2 intervals.*

4 Conclusions and Next Steps

In this study we have used a novel method for testing clouds and radiation output from the HARMONIE NWP model by testing the cloud cover and cloud physical parameters independently. In addition our use of measured SW radiation to verify the modelled clouds is an improved method compared to traditional verification using synoptic surface observations, where only the cloud cover is verified. When verifying the model only by means of cloud cover, all correctly forecast overcast cases are considered true, despite the fact that they can have wrong cloud water loads or effective radii. This is why the verification using the clear sky index and cloud water loads gives complementary verification information that previously has often been ignored. Using this approach, our results indicate that cloud water loads in HARMONIE are too high.

Using the clear sky index as a proxy for cloudiness has also highlighted the binary (on/off) cloud cover in HARMONIE where the cloud cover tends to be 0/8 (zero octa) or 8/8 (8 octa); a similar result to that by Perez et al. (2014). Such behaviour is unlike observed cloud cover.

Our experiments were designed to test the influence of cloud inhomogeneity factor and the Nielsen cloud optical scheme on the NWP forecasts. Both have the effect of reducing surface, near surface and lower atmosphere temperatures, which results in a slightly larger negative bias over the Irish domain. In light of the verification of the cloud water path, the cloud inhomogeneity factor offset the effect of the positive bias in cloud water path by effectively reducing the cloud water and ice loads used by the radiation scheme by 30%.

Further work will be carried out using MUSC to comprehensively test the influence of cloud condensate on radiation output compared to observations. The modelled cloud effective radius data

could also be compared to the corresponding MSGCPP product. The results presented here demonstrate the need for a collaborative effort between the radiation and the cloud working groups to resolve some of the issues outlined.

5 References

Brousseau P., Berre L., Bouttier F., and Desroziers G. Background-error covariances for a convective-scale data-assimilation system: AROME-France 3D-Var. Q.J.R. Meteorol. Soc., 137:409–422, 2011.

Cahalan, R. F., Ridgway, W., Wiscombe, W. J., Bell, T. L., & Snider, J. B. (1994). The albedo of fractal stratocumulus clouds. *Journal of the Atmospheric Sciences*, *51*(16), 2434-2455.

Dee, D. P., Uppala, S. M., Simmons, A. J., Berrisford, P., Poli, P., Kobayashi, S., Andrae, U., Balmaseda, M. A., Balsamo, G., Bauer, P., Bechtold, P., Beljaars, A. C. M., van de Berg, L., Bidlot, J., Bormann, N., Delsol, C., Dragani, R., Fuentes, M., Geer, A. J., Haimberger, L., Healy, S. B., Hersbach, H., Hólm, E. V., Isaksen, L., Kållberg, P., Köhler, M., Matricardi, M., McNally, A. P., Monge-Sanz, B. M., Morcrette, J.-J., Park, B.-K., Peubey, C., de Rosnay, P., Tavolato, C., Thépaut, J.-N. and Vitart, F. (2011), The ERA-Interim reanalysis: configuration and performance of the data assimilation system. Q.J.R. Meteorol. Soc., 137: 553–597. doi:10.1002/qj.828

Ebert, E.E. and Curry, J.A.: A parameterization of ice cloud optical properties for climate models, J. Geophys. Res., 97, 3834–3836, 1992.

ECMWF: IFS documentation – Cy38r1, Part IV: Physical processes, available at: http://old.ecmwf.int/research/ifsdocs/CY38r1/IFSPart4.pdf, 2012.

Fouquart, Y.: Radiative transfer in climate modeling, in: NATO Advanced Study Institute on Physically-Based Modeling and Simulation of Climate and Climatic Changes, edited by: Schlesinger, M. E., 223–283, 1987.

Fouquart, Y. and Bonnel, B.: Computations of solar heating of the earth's atmosphere – a new parameterization, Beitr. Phys. Atmos., 53, 35–62, 1980.

Fu, Q., Carlin, B., & Mace, G. (2000). Cirrus horizontal inhomogeneity and OLR bias. *Geophysical research letters*, *27*(20), 3341-3344.

Hess, M., Köpke, P., and Schult, I.: Optical properties of aerosols and clouds. The software package OPAC, B. Am. Meteorol. Soc., 79, 831–844, 1998.

Hogan, R.J., Personal communication regarding "The Effect of Cloud Structure on Radiation", by Anna Mary Townsend, B.Sc. Dissertation, University of Reading.

Hogan, R. J., & Illingworth, A. J. (2003). Parameterizing ice cloud inhomogeneity and the overlap of inhomogeneities using cloud radar data. *Journal of the atmospheric sciences*, *60*(5), 756-767.

Joseph, J.H., Wiscombe, W.J., and Weinman, J.A.: The Delta-Eddington approximation for radiative flux transfer, J. Atmos. Sci., 33, 2452–2459, 1976.

Laprise, R., 1992: The Euler equations of motion with hydrostatic pressure as an independent variable. Mon. Wea. Rev., 120, 197–207.

Mascart, P.J. and Bougeault, P.: The Meso-NH Atmospheric Simulation System: Scientific Documentation, Tech. rep., Meteo France, Toulouse, France, 2011.

Mayer, B. and Kylling, A.: Technical note: The libRadtran software package for radiative transfer calculations – description and examples of use, Atmos. Chem. Phys., 5, 1855–1877, doi:10.5194/acp-5-1855-2005, 2005.

Nielsen, K.P., Gleeson, E., and Rontu, L.: Radiation sensitivity tests of the HARMONIE 37h1 NWP model, Geosci. Model Dev., 7, 1433-1449, doi:10.5194/gmd-7-1433-2014, 2014.

Oreopoulos, L., & Cahalan, R. F. (2005). Cloud inhomogeneity from MODIS. *Journal of climate*, *18*(23), 5110-5124.

Daniel Martin Perez, Gema Morales Martin and Javier Calvo Sanchez, 2014: Statistical condensation scheme: Vertical variation of the saturation and convolution, ALADIN-HIRLAM Newsletter 3: 36.

Pomroy, H. R., & Illingworth, A. J. (2000). Ice cloud inhomogeneity: Quantifying bias in emissivity from radar observations. *Geophysical research letters*, *27*(14), 2101-2104.

Roebeling, R.A., A.J. Feijt, and P. Stammes (2006). Cloud property retrievals for climate monitoring: implications of differences between SEVIRI on METEOSAT-8 and AVHRR on NOAA-17, J. Geophys. Res., 111, 20210, doi:10.1029/2005JD006990.

Savijärvi, H., 1990: Fast Radiation Parameterization Schemes for Mesoscale and Short-Range Forecast Models. *J. Appl. Meteor.*, **29**, 437–447.
doi: http://dx.doi.org/10.1175/1520-0450(1990)029<0437:FRPSFM>2.0.CO;2

Scheirer, R., & Macke, A. (2003). Cloud inhomogeneity and broadband solar fluxes. *Journal of Geophysical Research: Atmospheres (1984–2012)*, *108*(D19).

Seity Y., Brousseau P., Malardel S., Hello G., Benard P., Bouttier F., Lac C. and Masson V. The AROME-France convective-scale operational model. Mon. Wea. Rev., 139:976–991, 2011.

Simmons, A., and D. M. Burridge, 1981: An energy and angular-momentum conserving finite-difference scheme and hybrid vertical coordinates. Mon. Wea. Rev., 109, 758–766.

Slingo, A.: A GCM parameterization for the shortwave radiative properties of water clouds, J. Atmos. Sci., 46, 1419–1427, 1989.

Stamnes, K., Tsay, S.-C., Wiscombe, W., and Jayaweera, K.: Numerically stable algorithm for discrete-ordinate-method radiative transfer in multiple scattering and emitting layered media, Appl. Optics, 27, 2502–2509, 1988.

Stamnes, K., Tsay, S.-C., and Laszlo, I.: DISORT, a GeneralPurpose Fortran Program for Discrete-Ordinate-Method Radiative Transfer in Scattering and Emitting Layered Media: Documentation and Methodology, Tech. rep., Stevens Insitute of Technology, Hoboken, NJ, USA, 2000.

Tegen, I., P. Hollrig, M. Chin, I. Fung, D. Jacob, and J. Penner, 1997: Contribution of different aerosol species to the global aerosol extinction optical thickness: Estimates from model results. J. Geophys. Res., 102, 23895-23915

Tiedtke, M. (1996). An extension of of cloud-radiation parameterization in the ecmwf model: The representation of sub-grid scale variations of optical depth. Mon. Wea. Rev.,124, 745-750.

Toll, V., Reis, K., Ots, R., Kaasik, M., Männik, A., Prank, M., & Sofiev, M. (2015). SILAM and MACC reanalysis aerosol data used for simulating the aerosol direct radiative effect with the NWP

model HARMONIE for summer 2010 wildfire case in Russia. *Atmospheric Environment*. http://dx.doi.org/10.1016/j.atmosenv.2015.06.007

Toll, V., Gleeson, E., Nielsen, K.P., Männik, A., Mašek, J., Rontu, L., Post, P., Importance of the direct radiative effect of aerosols in numerical weather prediction for the European region, In preparation.

Wyser, K., Rontu, L., and Savijärvi, H.: Introducing the effective radius into a fast radiation scheme of a mesoscale model, Contr. Atmos. Phys., 72, 205–218, 1999.

6 Acknowledgements

The authors would like to thank Noelle Gillespie, Chief Scientist, Valentia Observatory for providing shortwave radiation measurement data.